Available at www.ComputerScienceWeb.com
POWERED BY SCIENCE DIRECT®

Robotics and Autonomous Systems 45 (2003) 235–247

Robotics and Autonomous Systems

www.elsevier.com/locate/robot

Corridor navigation and wall-following stable control for sonar-based mobile robots

Ricardo Carelli [a,*], Eduardo Oliveira Freire [b,1]

[a] *Instituto de Automática, Universidad Nacional de San Juan, Av. San Martín Oeste 1109, 5400 San Juan, Argentina*
[b] *Departamento de Física da Universidade Federal de Sergipe, Av. Marechal Rondon, s/n, Jardim Rosa Elze, São Cristovão, SE, Brazil*

Received 5 June 2002; received in revised form 9 September 2003; accepted 17 September 2003

Abstract

In this paper, a mobile robot control law for corridor navigation and wall-following, based on sonar and odometric sensorial information is proposed. The control law allows for stable navigation avoiding actuator saturation. The posture information of the robot travelling through the corridor is estimated by using odometric and sonar sensing. The control system is theoretically proved to be asymptotically stable. Obstacle avoidance capability is added to the control system as a perturbation signal. A state variables estimation structure is proposed that fuses the sonar and odometric information. Experimental results are presented to show the performance of the proposed control system.

Keywords: Mobile robots; Autonomous navigation; Lyapunov stability; State estimation

1. Introduction

Mobile robots are mechanical devices capable of moving in an environment with a certain degree of autonomy. Autonomous navigation is associated to the availability of external sensors that capture information of the environment through visual images or distance or proximity measurements. The most common sensors are distance sensors (ultrasonic, laser, etc.) capable of detecting obstacles and of measuring the distance to walls close to the robot path. When advanced autonomous robots navigate within indoor environments (industrial or civil buildings), they have to be endowed the ability to move through corridors, to follow walls, to turn corners and to enter open areas of the rooms.

As regards the corridor and wall-following navigation problem, some control algorithms based on artificial vision have been proposed. In [10], image processing is used to detect perspective lines to guide the robot along the centre axis of the corridor. In [17], perspective lines on the ceiling are used for vehicle localization in corridors. Other authors have proposed to use the so-called optic flow to guide the robot through corridors. In [13], two lateral cameras mounted on the robot are used, and the optical flow is computed to compare the apparent image velocity on

* Corresponding author. Fax: +54-264 421 3672.
E-mail addresses: rcarelli@inaut.unsj.edu.ar (R. Carelli), eofreire@yahoo.com.br (E. Oliveira Freire).
[1] Fax: +55-79 212 6807.

0921-8890/$ – see front matter © 2003 Elsevier B.V. All rights reserved.
doi:10.1016/j.robot.2003.09.005

both cameras in order to control robot motion. In [6,7], one camera is used to drive the robot along the corridor axis or to follow a wall, by using optic flow computation and its temporal derivatives. In [2], a globally stable control algorithm for wall-following based on incremental encoders and one sonar sensor is developed. Excepting for a few cases, as in the last-cited paper, the proposed controllers do not include any stability analysis that considers the non-linear model of the mobile robot.

In this paper, a control algorithm is developed to guide a mobile robot along a corridor or to allow the robot to follow a wall. The algorithm is based on distance measurements supplied by sonar sensors and it is designed to be asymptotically stable and to avoid saturation of robot actuators. The robot states are obtained by estimation with an extended information filter (EIF) [12], with adaptive covariance based on empirical rules. Experimental results are presented to show the performance of the proposed controller.

The paper is organized as follows. Section 2 gives the well-known kinematics of unicycle-like mobile robots. Section 3 presents the proposed corridor navigation controller as well as the stability analysis of the control system. A description is also given on how the corridor navigation controller can be adapted to wall-following tasks. Section 4 explains the algorithm that is used to give the robot the obstacle avoidance capability. Section 5 presents the proposed strategy for estimating the robot state variables to feed the control algorithm. Section 6 presents the experimental results and Section 7 states some concluding remarks.

2. Kinematics equations

Let us consider the unicycle-like robot positioned at a non-zero distance from a goal point $\mathbf{x}_\mathrm{d}$ in a fixed Cartesian frame. Its motion towards $\mathbf{x}_\mathrm{d}$ is governed by the combined action of both the angular velocity ω and the linear velocity $\mathbf{u}$, which is always on the direction of one of the axes of frame $\langle a\rangle$ attached to the robot, as depicted in Fig. 1. Then, the usual set of kinematics equations, which involves Cartesian position $[\ x \quad y\ ]^\mathrm{T}$ of the vehicle and its heading φ, are

$$\dot{x} = u\cos\varphi, \qquad \dot{y} = u\sin\varphi, \qquad \dot{\varphi} = \omega, \tag{1}$$

where u is the magnitude of the linear velocity vector and φ is measured with respect to the x-axis.

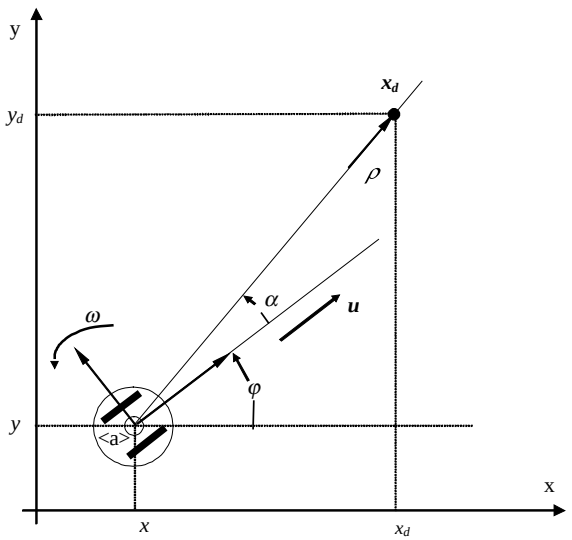

Fig. 1. Vehicle position and heading.

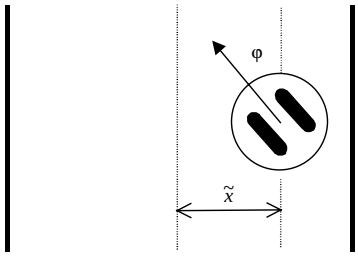

Fig. 2. The robot in the corridor.

Now, let us consider the case of a robot navigating in a corridor. The state variables are thus defined in relation to the corridor as $\tilde{x}$ and φ, where $\tilde{x}$ represents the deviation of the robot from the corridor centre-line (or the desired corridor line) and φ is the angular deviation as related to the corridor axis, as shown in Fig. 2. In this case, the kinematics equations are reduced to

$$\dot{\tilde{x}} = u \sin\varphi, \qquad \dot{\varphi} = \omega. \tag{2}$$

3. Controller design

Let us assume the mobile robot moving along the corridor is described by the kinematics equations (2). Then, the control objective is to design control actions $\omega(t)$ and $u(t)$ such that the control errors $\tilde{x}(t)$ and $\varphi(t)$ tend asymptotically to zero while maintaining the control actions within specified bounds. The following control law is proposed, based on the measurement of error variables $\tilde{x}(t)$ and $\varphi(t)$

$$u = u(\varphi, \tilde{x}), \quad u \geq 0, \qquad \omega = -k_{\varphi}(\varphi)\varphi - k_{\tilde{x}}(\tilde{x})\tilde{x}u\frac{\sin\varphi}{\varphi}, \tag{3}$$

where $k_{\varphi}(\varphi)$ and $k_{\tilde{x}}(\tilde{x})$ are the suitably selected positive functions – which are defined at the end of this section – in order to avoid saturation of control command ω. The closed-loop equation from (2) and (3) is

$$\dot{\tilde{x}} = u \sin\varphi, \qquad \dot{\varphi} = -k_{\varphi}(\varphi)\varphi - k_{\tilde{x}}(\tilde{x})\tilde{x}u\frac{\sin\varphi}{\varphi}. \tag{4}$$

In (4), the only equilibrium state is $[\,\tilde{x} \quad \varphi\,]^{\mathrm{T}} = 0$. Now, consider the following Lyapunov candidate function

$$V = \frac{\varphi^2}{2} + \int_0^{\tilde{x}} k_{\tilde{x}}(\eta)\eta\,\mathrm{d}\eta. \tag{5}$$

This positive definite function represents the summation of potential energies from heading and position errors of the robot in the corridor. Moreover, $k_{\tilde{x}}(\cdot)$ is selected as in [11]

$$k_{\tilde{x}}(\tilde{x}) \geq \alpha(|\tilde{x}|) \quad \forall\tilde{x} \in \Re,$$

where $\alpha(\cdot)$ is a function of class K [16]. Then, it can be proved that the integral term in V is radially unbounded. Therefore, it can be concluded that V is a globally positive definite and radially unbounded function.

The time derivative of the Lyapunov function candidate is

$$\dot{V}(\tilde{x}, \varphi) = \varphi\dot{\varphi} + k_{\tilde{x}}(\tilde{x})\tilde{x}\dot{\tilde{x}},$$

where the Leibnitz' rule has been used for differentiation of integrals. By substituting the closed-loop equation (4)

$$\dot{V}(\tilde{x},\varphi) = \varphi\left\{-k_\varphi(\varphi)\varphi - k_{\tilde{x}}(\tilde{x})\tilde{x}u\frac{\sin\varphi}{\varphi}\right\} + k_{\tilde{x}}(\tilde{x})\tilde{x}u\sin\varphi, \qquad \dot{V}(\tilde{x},\varphi) = -k_\varphi(\varphi)\varphi^2 \leq 0. \tag{6}$$

Eq. (6) represents a semi-definite negative function, and it can be concluded that state variables $\tilde{x}, \varphi$ are bounded and φ is a square-integrable time function.

To prove the asymptotic stability, we exploit the autonomous nature of the closed-loop system (4) in order to apply the Krasovskii–LaSalle's theorem [16]. In the region

$$\Omega = \left\{\begin{bmatrix}\tilde{x}\\ \varphi\end{bmatrix} : \dot{V}(\tilde{x},\varphi) = 0\right\} \Rightarrow \left\{\begin{bmatrix}\tilde{x}\\ \varphi\end{bmatrix} = \begin{bmatrix}\tilde{x}\\ 0\end{bmatrix}\right\},$$

the only invariant is $\tilde{x} = 0$. Therefore, by invoking LaSalle's theorem, it can be concluded that the origin of the state space is globally uniformly asymptotically stable.

In a similar way as proposed in [11], the following definition for $k_\varphi(\varphi)$, $k_{\tilde{x}}(\tilde{x})$ functions is considered

$$k_\varphi(\varphi) = \frac{k_1}{a_1 + |\varphi|}, \qquad k_{\tilde{x}}(\tilde{x}) = \frac{k_2}{a_2 + |\tilde{x}|}, \tag{7}$$

where k_1, k_2, a_1 and a_2 are the positive constants. These functions verify that

$$k_\varphi(\varphi) > 0, \qquad k_{\tilde{x}}(\tilde{x}) \geq \alpha(|\tilde{x}|) \quad \forall\tilde{x} \in \Re,$$

which have been assumed in the stability proof. On the other hand, from (3), the absolute value of the control action ω is

$$|\omega| \leq k_1\left|\frac{\varphi}{a_1 + |\varphi|}\right| + k_2\left|\frac{\tilde{x}u}{a_2 + |\tilde{x}|}\right|.$$

Since $|x/(a + |x|)| \leq 1$ for all $x \in \Re, a > 0$

$$|\omega| \leq k_1 + k_2 u_\mathrm{d}, \tag{8}$$

where u_d is given in (9), and it represents the maximum desirable value for linear velocity u. If we choose k_1, k_2 so that $k_1 + k_2 u_\mathrm{d} \leq \omega_\mathrm{max}$ with ω_max the maximum admissible value for $|\omega|$, then the controller guarantees that $|\omega| \leq \omega_\mathrm{max}$ for all $t \geq 0$.

Finally, the linear velocity can be taken as constant, $u(\varphi,\tilde{x}) = u_\mathrm{d}$. However, a cautious and smooth behaviour for the robot can be attained as a function of the control errors, by regarding the function

$$u(\varphi,\tilde{x}) = (u_\mathrm{d} - k|\tilde{x}|)\cos\varphi, \quad k > 0, \tag{9}$$

where u_d is the steady-state linear velocity and k is taken such that $u(\varphi,\tilde{x}) > 0$ for all $\varphi, \tilde{x}$ within a physically valid range.

3.1. Wall-following motion

If a different set of state variables is considered, it is possible to use the corridor navigation controller to enable the robot to follow a wall. This is possible because the two tasks are very similar to each other. In this case, the state variables are defined in relation to the wall as φ and $\tilde{d}$, where φ is the angular deviation relative to the wall line, and $\tilde{d}$ represents the distance of the robot from an imaginary line at a desired distance d_wall from the wall, as depicted in Fig. 3. In this figure, a typical ultrasonic arrangement on the mobile robot is represented, with each ultrasonic sensor named as s_i. In this case, variable $\tilde{d}$ can be calculated through the following equation:

$$\tilde{d} = \pm\{d_\mathrm{wall} - \min(\tfrac{1}{2}(y_{S_0} + y_{S_{15}})), (\tfrac{1}{2}(y_{S_7} + y_{S_8}))\}, \tag{10}$$

where minus sign is considered if the wall being followed is at the robot's right side.

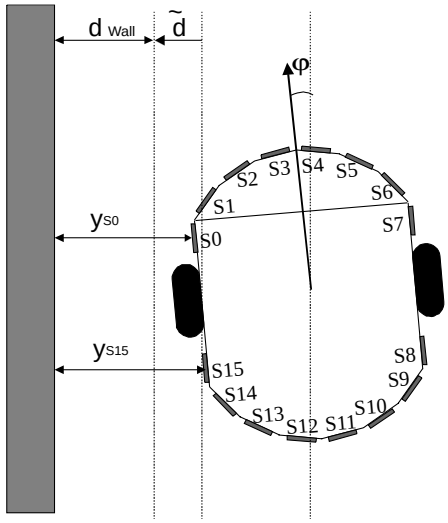

Fig. 3. State variables for wall-following control.

4. Obstacle avoidance

The controller can be endowed the additional capability of avoiding obstacles that may eventually appear on the robot's path along the corridor or when the robot is following a wall. To this purpose, we consider a deviation signal as an additive perturbation ω_p to the control command, as shown in Fig. 4. The deviation control signal ω_p will steer the robot in order to avoid the obstacle. This signal is calculated based on the positioning controller developed in [5,15]. This controller is capable of guiding the robot from an initial point to a destination point $\mathbf{x}_d$ as shown in Fig. 1. The algorithm is adapted to the obstacle avoidance in the context of corridor navigation, by placing the destination point at a constant distance (1 m in the experiences) away from the robot and on the direction it is pointing at each instant (Fig. 5). Thus, the algorithm will have no effect on the robot drive if no obstacle is detected. Nevertheless, while detecting an obstacle in the robot-working environment, it momentarily shifts the target position to a new destination point $\mathbf{x}_r$ rotated an angle ψ, as it can be seen in Fig. 5, which generates a deviation command

$$\omega_p = k_\psi \psi + \gamma \sin\psi \cos\psi. \tag{11}$$

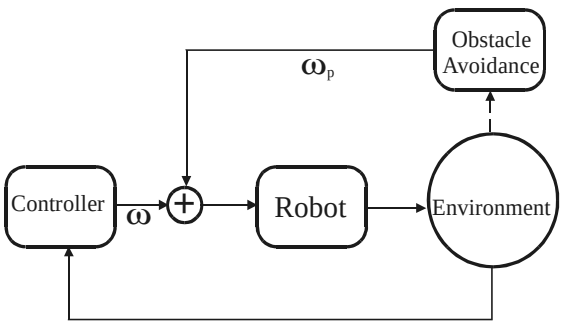

Fig. 4. Adding the obstacle avoidance capability.

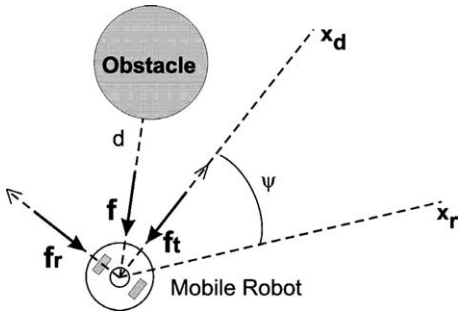

Fig. 5. The fictitious force **f** on the mobile robot.

Eq. (11) is taken from [5,15], where k_ψ and γ are the positive design constants. Besides, the linear velocity command $u(\varphi, \tilde{x})$ of Eq. (9) is re-defined to generate a cautious motion when steering to avoid an obstacle

$$u_{\text{new}} = [u(\varphi, \tilde{x})] \cos \psi.$$

The way of calculating angle ψ is presented now, based on an extended impedance concept [5]. To this aim, an interaction fictitious force **f** is generated as a function of the robot–obstacle distance d, as shown in Fig. 5. Force **f** represents a virtual interaction between the robot and the obstacle with two components: a longitudinal component on the robot heading direction $\mathbf{f}_\text{t}$, and a perpendicular component $\mathbf{f}_\text{r}$.

The magnitude of force **f** is calculated as [3]:

$$f = a - b(d - d_{\min})^2, \tag{12}$$

where a and b are the positive constants, such that $a - b(d_{\max} - d_{\min})^2 = 0$; the value $d_{\max}$ is the maximum distance between the robot and the detected obstacle that should produce a repulsion force **f**, $d_{\min}$ the minimum distance that the sensorial system is able to measure, and d the distance measured between the robot and the obstacle. Desired interaction impedance is now defined [5,15] as the linear dynamic relationship

$$Z(p) = Bp + K, \qquad p = \frac{\mathrm{d}}{\mathrm{d}t}, \tag{13}$$

where B and K are the positive constants. Constant B represents a damping effect, and K a spring effect in the virtual interaction between the mobile robot and the obstacle. An auxiliary variable $x_\text{a}(t)$

$$x_\text{a}(t) = Z^{-1}(p)\mathbf{f}_\text{t} \tag{14}$$

is now used to generate the rotation angle ψ of the target point with respect to the vehicle centre

$$\psi = x_\text{a} \operatorname{sign}(\mathbf{f}_\text{r}). \tag{15}$$

Then, the rotation transform

$$\mathbf{x}_\text{r} = \begin{bmatrix} \cos\psi & \sin\psi \\ -\sin\psi & \cos\psi \end{bmatrix} \mathbf{x}_\text{d}$$

is applied to calculate the new target point $\mathbf{x}_\text{r}$ (Fig. 5).

In short, on account of the fictitious resultant force, the destination point of the robot is shifted and, then, a convenient deviation command ω_p is generated, allowing the robot to steer and avoid the detected obstacle. The reaction capability of the robot to avoid the obstacle is regulated by a proper selection of constants in Eqs. (11)–(13). This way, the algorithm can be applied to the corridor- or wall-following navigation with obstacle avoidance capability. It has to be noted that, when no obstacle is present within a maximum distance $d_{\max}$ from the robot, ψ is

zero and no obstacle avoidance signals are added to the control commands. Therefore the robot evolves according to the control objective described in Section 3.

5. State variables estimation

The controller is required to be backfed with the values of states $\tilde{x}(t)$ and $\varphi(t)$ at each instant. These values can be primarily obtained from sonar measurements. Fig. 6 shows a typical situation where lateral sonar sensors S_0, S_{15}, S_7, and S_8 are used. For this case, the following equations allow calculating the state variables

$$d_{\text{left}} = \tfrac{1}{2}(y_{S_0} + y_{S_{15}}), \qquad d_{\text{right}} = \tfrac{1}{2}(y_{S_7} + y_{S_8}), \tag{16}$$

$$\text{diff} = \tfrac{1}{2}((y_{S_0} - y_{S_{15}}) + (y_{S_7} - y_{S_8})), \tag{17}$$

$$\varphi = \sin^{-1}\left(\frac{\text{diff}}{d}\right), \qquad \tilde{x} = \frac{d_{\text{right}} - d_{\text{left}}}{2}. \tag{18}$$

Sonar measurements may deteriorate or be impossible to obtain under certain circumstances as, for example, when the robot is travelling close to an open door in the corridor, or when the robot has a significant angle of deviation from the corridor axis. The latter condition originates from the fact that a sonar sensor collects useful data only when its direction orthogonal to the reflecting surface lies within the beam width of the receiver, thus allowing for wall detection only for a restricted heading range [2]. The range for this angle is approximately $\varphi = 17^\circ$ for the electrostatic sensors in the robot used in the experiences. On this account, it is important to consider other measurements as well, such as the odometric data provided by the robot. The fusion of these data using optimal filters produces optimal estimations of the robot states, thus minimizing the uncertainty in the sensor measurements. Some authors, as in [14], have fused the odometric and sonar data. Here, we propose to fuse the sonar measurements $\tilde{x}_1$, φ_1 and an updated odometric measurements $\tilde{x}_2$, φ_2, by using a *decentralized information filter* [9,12], as represented in Fig. 7. The *information filter* [12] is essentially a Kalman filter [4], but it is expressed in terms of measurements of information relative to some states of interest. The information filter has two major advantages over a Kalman filter [12]. First, the initialization of the information filter (definition of the initial value of the state information vector) is straightforward, while the initialization of the Kalman filter depends on previous knowledge of the system or even on some chance trial. Second, the information filter equations are simpler than the equivalent Kalman filter equations. A decentralized version of the information filter, the *decentralized information filter*, is here adopted,

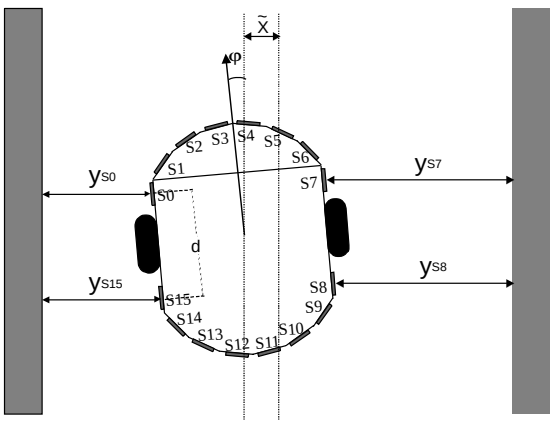

Fig. 6. Calculation of state variables from distance measurements.

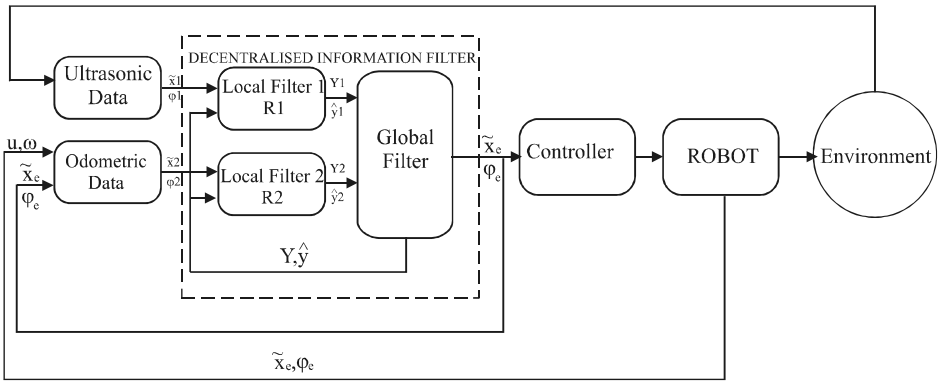

Fig. 7. Fusion of odometric and sonar measurements.

once it avoids using matrix operations, thus allowing a faster calculation. As shown in Fig. 7, the number of local filters is chosen according to the number of data sources involved in the fusion process (ultrasonic data and updated odometric data in this case). The output of the decentralized information filter, $\tilde{x}_e$, φ_e, is also used to update the odometric data.

The inputs to the *Odometric Data* block in Fig. 7 are the linear and angular velocities of the robot and the estimated state variables. This block performs the following calculation at each sampling step to update states based in odometric data $\tilde{x}_2$, φ_2.

Odometry updating:

$$\tilde{x}_2(k-1) = \tilde{x}_e(k-1), \qquad \varphi_2(k-1) = \varphi_e(k-1). \tag{19}$$

New state variables based on odometric data (refer to kinematics equations (2)):

$$\tilde{x}_2(k) = \tilde{x}_2(k-1) + u(k)\,\Delta t \sin(\varphi_2(k)), \qquad \varphi_2(k) = \varphi_2(k-1) + \omega(k)\,\Delta t, \tag{20}$$

where $u(k)$ and $\omega(k)$ are the linear and angular velocities of the robot at instant t_k, and Δt is the sampling time in the discrete-time implementation.

5.1. The information filter

Let us suppose a system whose model is stated as

$$\mathbf{x}(k) = \boldsymbol{\varphi}(k)\mathbf{x}(k-1) + \mathbf{w}(k), \qquad \mathbf{z}(k) = \mathbf{H}(k)\mathbf{x}(k) + \mathbf{v}(k), \tag{21}$$

where $\mathbf{x}(k)$ is the system state vector at time t_k, $\boldsymbol{\varphi}(k)$ the system matrix, $\mathbf{z}(k)$ the observation vector at time t_k, $\mathbf{H}(k)$ the observation matrix, $\mathbf{w}(k)$ the vector representing the noise on the system and $\mathbf{v}(k)$ represents the measurement noise. Vectors $\mathbf{w}(k)$ and $\mathbf{v}(k)$ represent white uncorrelated noise sequences with covariance matrices $\mathbf{Q}$ and $\mathbf{R}$, respectively.

The standard notation $\hat{\mathbf{x}}(k|k-1)$ is used to indicate the estimate of the system state vector at time t_k based on the knowledge about the process obtained until the instant t_{k-1}.

The *information filter* equations [12] are given in the following:

- Information matrix:

$$\mathbf{Y}(k) = \mathbf{P}^{-1}(k), \tag{22}$$

where $\mathbf{P}$ is the matrix of the covariance error between the real state $\mathbf{x}(k)$ and the estimated state $\hat{\mathbf{x}}(k)$.

- State information vector:

$$\hat{\mathbf{y}}(k) = \mathbf{P}^{-1}(k)\hat{\mathbf{x}}(k) = \mathbf{Y}(k)\hat{\mathbf{x}}(k). \tag{23}$$

- Prediction equations:

$$\hat{\mathbf{y}}(k|k-1) = \mathbf{L}(k|k-1)\hat{\mathbf{y}}(k-1|k-1), \qquad \mathbf{Y}(k) = [\boldsymbol{\varphi}(k)\mathbf{Y}^{-1}(k-1|k-1)\boldsymbol{\varphi}^{\mathrm{T}}(k) + \mathbf{Q}(k)]^{-1}. \tag{24}$$

- Estimation equations:

$$\hat{\mathbf{y}}(k) = \hat{\mathbf{y}}(k|k-1) + \mathbf{i}(k), \qquad \mathbf{Y}(k) = \mathbf{Y}(k|k-1) + \mathbf{I}(k). \tag{25}$$

In the above equations, the information propagation coefficient $\mathbf{L}(k|k-1)$, the information state contribution $\mathbf{i}(k)$ from an observation $\mathbf{z}(k)$, and its associated information matrix $\mathbf{I}(k)$ are respectively given by

$$\begin{aligned} &\mathbf{L}(k|k-1) = \mathbf{Y}(k|k-1)\boldsymbol{\varphi}(k)\mathbf{Y}^{-1}(k-1|k-1), \\ &\mathbf{i}(k) = \mathbf{H}^{\mathrm{T}}(k)\mathbf{R}^{-1}(k)\mathbf{z}(k), \qquad \mathbf{I}(k) = \mathbf{H}^{\mathrm{T}}(k)\mathbf{R}^{-1}(k)\mathbf{H}(k). \end{aligned} \tag{26}$$

Eq. (25) shows that at each sampling instant, the estimation of the state information vector $\hat{\mathbf{y}}(k)$ is given by the prediction of the state information vector at instant k, based on the information available until instant $k-1$, plus the contribution of the current state information $\mathbf{i}(k)$. It also states that the information matrix at the current instant k, $\mathbf{Y}(k)$, is given by the prediction of the information matrix at instant k, based on the information available until instant $k-1$, plus the information matrix at instant k.

There are two approaches to implement a *decentralized filter*. In the first one, the filter should be implemented using more than one processing unit [12]. In the second approach, the decentralized filter consists of a global filter and several local filters implemented in the same processing unit. The *decentralized Kalman filter* and the *decentralized information filter* presented in [12] follow the first approach, while the *decentralized Kalman filter* presented in [4] follows the second one. As the robot used in the experiments is controlled by only one processor, the decentralized information filter considered here follows the second approach and has been proposed by the authors in [9]. Its structure can be seen in Fig. 7, and the mathematical formulation is given as follows:

- For the local filters:

$$\hat{\mathbf{y}}_i(k) = \hat{\mathbf{y}}(k-1) + \mathbf{i}_i(k), \qquad \mathbf{Y}_i(k) = \mathbf{Y}(k-1) + \mathbf{I}_i(k), \tag{27}$$

where $\mathbf{i}_i(k)$ and $\mathbf{I}_i(k)$ are calculated for each local filter using Eq. (26).

- For the global filter:

$$\hat{\mathbf{y}}(k) = \sum_{i}^{n} \hat{\mathbf{y}}_i(k) - (n-1)\hat{\mathbf{y}}(k-1), \qquad \mathbf{Y}(k) = \sum_{i=1}^{n} \mathbf{Y}_i(k) - (n-1)\mathbf{Y}(k-1), \tag{28}$$

where n is the number of local filters.

In our particular application, the system model is that stated in Eq. (21) with $\mathbf{H}(k) = \mathbf{I}$, $\boldsymbol{\varphi}(k) = \mathbf{I}$, $\mathbf{w}(k) = 0$, and then $\mathbf{Q}(k) = \mathbf{0}$. The covariance associated to each local information filter can be defined by using different methods, considering the data provided by the robot sensors. The more reliable a certain sensor is, the lower the covariance associated to its data. A satisfactory way to calculate such covariance is based on fuzzy logic, which is the method adopted in this work. Following this approach, the linguistic variables are used to express the designer's knowledge about the robot navigation system and the robot's working environment into a rule base [8]. Two input fuzzy variables (antecedents) are used: the product of left and right distance ($d_{\mathrm{left}} \times d_{\mathrm{right}}$), and diff (Eqs. (16) and (17)). The reason for choosing these variables is that, for openings to corridor branches and to open doors along the corridor (indicated by the a large product $d_{\mathrm{left}} \times d_{\mathrm{right}}$), or for large robot heading deviations from the corridor

Table 1
Fuzzy rules[a]

Diff × d_{left} × d_{right}	S	L
VS	R1 = VS, R2 = VL	R1 = L, R2 = S
S	R1 = VS, R2 = VL	R1 = VL, R2 = VS
L	R1 = L, R2 = S	R1 = VL, R2 = VS
VL	R1 = VL, R2 = VS	R1 = VL, R2 = VS

[a] VS: very small; S: small; L: large; VL: very large; R1: covariance of ultrasonic data; R2: covariance of odometric data.

axis (indicated by a large value of diff), the ultrasonic measurements should be considered as not reliable, and the covariance associated to the ultrasonic data should be large as well, thus making this measurement less relevant to the output of the information filter. Under this condition, the odometric data dominate the information filter output. On the other hand, when there are walls on both sides of the corridor and the deviation-heading angle of the robot from the corridor axis is small, the ultrasonic data dominate the filter output. The consequents of the fuzzy logic are the covariances associated to the local information filters receiving the data from the updated odometry and from the sonar sensors, and they are modelled as singletons [1]. Membership functions are taken as equally spaced symmetric triangle-shaped functions in each input fuzzy variable. Table 1 shows the fuzzy rules that are used to determine the covariance matrices. Defuzzyfication is made using the fuzzy mean method [1].

The output of the global filter is now the input to the controller, and it is also used to update the odometric data as represented in Fig. 7.

6. Experimental results

Various experiments have been carried out to demonstrate the theoretical results and to show the performance of the control system. In these experiments, the controllers and the state estimation structure proposed in the previous sections have been used. Some improvement in the state estimation was achieved by adding a state estimation based on an extended information filter [12], whose inputs are the outputs from the decentralized information filter of Fig. 7. The laboratory experiments have been developed using a Pioneer II-DX mobile robot from Active Media. This robot is equipped with a ring of eight front- and eight rear-sonar sensors.

The first experiment consists of navigating along a corridor at the Institute of Automatics, National University of San Juan, Argentina. The corridor is 1.40 m wide and 20 m long, featuring several obstacles on the robot path, a local narrowing of the corridor to 1.20 m and local lateral openings to corridor branches and to open doors along the path. The controller includes the obstacle avoidance capability described in Section 4. The following controller specifications and design constants have been used in the experiment: $\omega_{max} = \pi/31$/s, $a_1 = a_2 = 2$, $k_1 = k_2 = 0.8$, $u_d = 0.3$ m/s. Fig. 8 shows the path followed by the robot along the corridor. The grey points

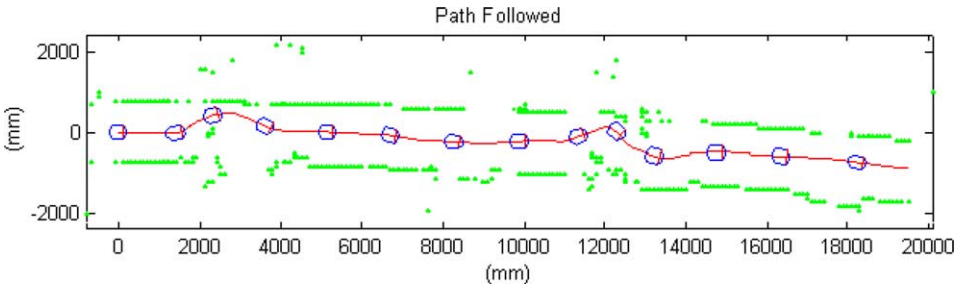

Fig. 8. The actually followed path along the corridor.

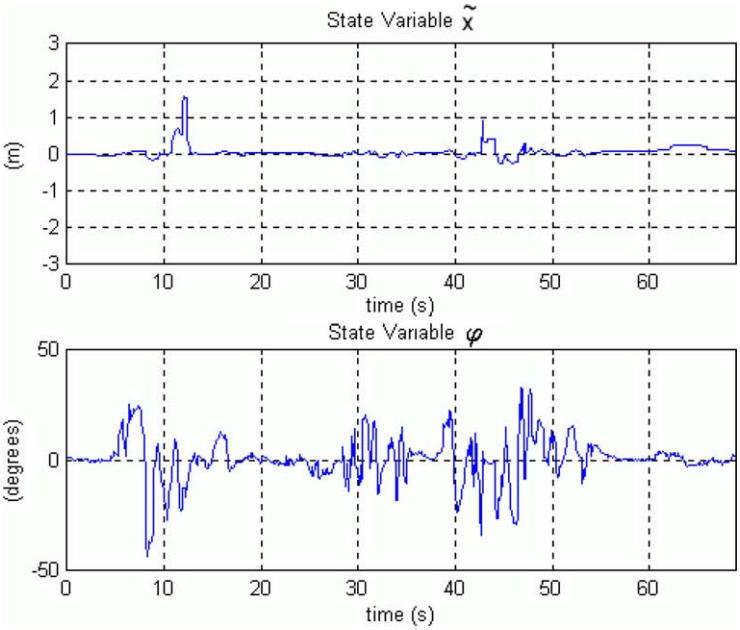

Fig. 9. Estimated state variables $\tilde{x}$, φ.

represent a reconstruction of the environment using ultrasonic data. In this figure – and later in Fig. 10 – a robot is depicted every 5 s starting at $t = 0$ s.

Fig. 9 shows the estimated state variables $\tilde{x}$, φ used by the controller—the estimation was made as described in Section 5. The transitions in these state variables evolution are related to obstacle avoidance manoeuvres and to the

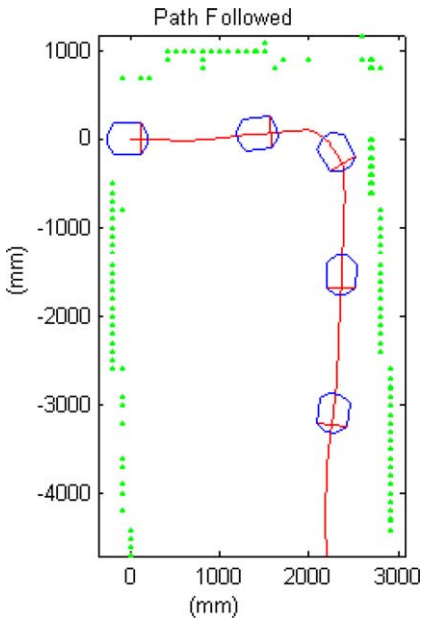

Fig. 10. Wall-following navigation task.

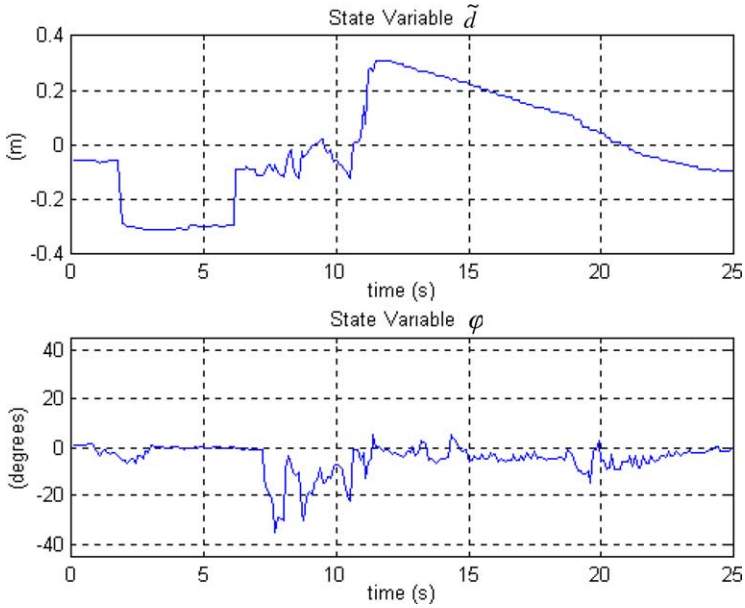

Fig. 11. Estimated state variables $\tilde{d}$, φ.

variables estimation process, due to problems that usually arise with ultrasonic echo reflections when the ultrasonic sensors are not well oriented during robot manoeuvres, and when open doors and cross corridors appear along the navigation corridor.

The second experiment is designed to show the performance of the controller when performing a wall-following navigation task. In this experiment, the robot starts following a wall at a desired 50 cm distance to its right side, and it reaches a second corner wall in front of it. The robot then avoids the wall as an obstacle by turning right, and then detects the wall on its left side again. Thus the robot positions itself until it reaches a 50 cm desired distance from the wall. Fig. 10 shows the evolution of the robot in this experiment. Again, the grey points represent a reconstruction of the environment using the ultrasonic measurements. The following controller specifications and design constants were used in the experiment: $\omega_{\max} = \pi/31$/s, $a_1 = a_2 = 2$, $k_1 = k_2 = 0.8$, $u_{\mathrm{d}} = 0.3$ m/s.

Fig. 11 shows the estimated state variables $\tilde{d}$, φ used by the controller (the estimation was made as described in Section 5).

Figs. 8 and 10 show that, even with non-smooth state variables estimations, as shown in Figs. 9 and 11, the proposed control system is able to smoothly and successfully guide the robot along a corridor or following a wall while avoiding obstacles.

7. Conclusions

A controller for guiding mobile robots in performing corridor navigation and wall-following tasks based on distance measurements has been presented. The resulting control system has been proven to be asymptotically stable and to avoid saturation of commands by keeping the angular velocity control action within specified limits. The state of the robot in the corridor or with respect to a near wall (lateral and angular deviations) is estimated from the odometric and sonar measurements. Obstacle avoidance capability has been added to the control by generating a perturbation signal, which is added to the control commands. The control system has been shown to work properly under experimental conditions, navigating along the corridors while successfully avoiding obstacles set in its path.

References

[1] R. Babuska, Fuzzy Modelling for Control, Kluwer Academic, USA, 1998.
[2] R. Benporad, M. Di Marco, A. Tesi, Wall-following controllers for sonar-based mobile robots, in: Proceedings of the 36th IEEE Conference on Decision and Control, San Diego, (A) December 1997.
[3] J. Borenstein, Y. Koren, The vector field histogram—fast obstacle avoidance for mobile robots, IEEE Transactions on Robotics and Automation 7 (3) (1991) 278–288.
[4] R. Brown, P. Hwang, Introduction to Randon Signals and Applied Kalman Filtering, 3rd Ed., Wiley, New York, USA, 1997.
[5] R. Carelli, H. Secchi, V. Mut, Algorithms for stable control of mobile robots with obstacle avoidance, Latin American Applied Research 29 (3/4) (1999) 191–196.
[6] R. Carelli, C. Soria, O. Nasisi, E. Freire, Stable AGV corridor navigation with fused vision-based control signals, in: Proceedings of the 28th Conference of the IEEE Industrial Electronics Society, IECON, Sevilla, Spain, November 5–8, 2002.
[7] A. Dev, B. Kröse, F. Groen, Navigation of a mobile robot on the temporal development of the optic flow, in: Proceedings of the IEEE/RSJ/GI International Conference on Intelligent Robots and Systems IROS'97, Grenoble, September 1997, pp. 558–563.
[8] E.O. Freire, T.F. Bastos-Filho, M. Sarcinelli-Filho, R. Carelli, O. Nasisi, A new mobile robot control architecture via control output fusion, in: Proceedings of the XV IFAC World Congress, Barcelona, Spain, July 21–26, 2002.
[9] E. Freire, R. Carelli, V. Mut, C. Soria, T.F. Bastos-Filho, M. Sarcinelli-Filho, Mobile robot navigation based on the fusion of control signals form different controllers, in: European Control Conference, ECC'2001, Porto, Portugal, September 4–7, CD Proceedings.
[10] R. Frizera Vassallo, H.J. Schneebeli, J. Santos-Victor, Visual navigation: combining visual servoing and appearance based methods, in: Proceedings of the International Symposium on Intelligent Robotic Systems, SIRS'98, Edinburgh, Scotland, July 1998.
[11] R. Kelly, R. Carelli, A class of nonlinear PD-type controllers for robot manipulators, Journal of Robotic Systems 13 (12) (1996) 793–802.
[12] A.G.O. Mutambara, Decentralized Estimation and Control for Multisensor Systems, CRC, Boca Raton, FL, 1998.
[13] J. Santos-Victor, G. Sandini, F. Curotto, S. Garibaldi, Divergent stereo in autonomous navigation: from bees to robots, International Journal of Computer Vision 14 (1995) 159–177.
[14] J.Z. Sasiadek, P. Hartana, Odometry and sonar data fusion for mobile robot navigation, in: Proceedings of the Sixth IFAC Symposium on Robot Control, SYROCO'00, vol. II, Vienna, Austria, September 21–23, 2000, Preprints, pp. 531–536.
[15] H. Secchi, R. Carelli, V. Mut, Discrete stable control of mobile robots with obstacle avoidance, in: Proceedings of the International Conference on Advanced Robotics, ICAR'01, Budapest, Hungary, August 22–25, 2001, pp. 405–411.
[16] M. Vidyasagar, Nonlinear Systems Analysis, 2nd Ed., Prentice-Hall, Englewood Cliffs, NJ, 1993.
[17] Z.F. Yang, W.H. Tsai, Viewing corridors as right parallelepipeds for vision-based vehicle localization, IEEE Transactions on Industrial Electronics 46 (3) (1999).

Ricardo Carelli (M'76–SM'98) was born in San Juan, Argentina in 1952. He graduated in Electrical Engineering from the National University of San Juan, Argentina, and received the Ph.D. degree in Electrical Engineering from the National University of Mexico (UNAM).

He is currently full Professor at the National University of San Juan and Independent Researcher of the National Council for Scientific and Technical Research (CONICET, Argentina). He is Adjunct Director of the Instituto de Automática, National University of San Juan. He also coordinates the Ph.D. and Master Programs in Control Engineering at the same university. His research interests are robotics, manufacturing systems, adaptive control and artificial intelligence applied to automatic control. Prof. Carelli is also a member of the Argentine Association of Automatic Control (AADECA-IFAC).

Eduardo Oliveira Freire was born in Aracaju, SE, Brazil, in December 1972. He received the degree of Electrical Engineering from the Federal University of Paraíba, Campina Grande, PB, Brazil, in 1995, and the Master and Doctorate degrees in Electrical Engineering from the Federal University of Espírito Santo, Vitória, ES, Brazil, in 1997 and 2002, respectively.

He is currently an Associate Professor with the Department of Physics of the Federal University of Sergipe, Aracaju, SE, Brazil. From 1999 to 2003 he was an Associate Professor with the University Tiradentes. His research interests are in mobile robot navigation and sensor fusion.